Multi-user transmission for the joint radar communication systems based on amplitude phase shift keying modulation and waveform diversity

Abdulmuneem Alselwi[1] , Adnan Umar Khan[1], Ijaz Mansoor Qureshi[2], Wasim Khan[1] and Abdul Basit[1]

[1]Faculty of Engineering and Technology, International Islamic University, Islamabad 44000, Pakistan and [2]Department of Electrical Engineering, Air University, Islamabad 44000, Pakistan

Abstract

In this paper, an efficient dual function radar-communication system is proposed to improve the system's resource utilization. In this work, we considered a scenario where the location of the communication receiver is known prior but the radar target is moving and its location is changing with time. Therefore, we proposed a closed-loop design that allows an adaptive selection of appropriate information embedding strategies during tracking operations. We used two strategies that utilize the amplitudes and/or phases of the transmitted radar waveforms toward the communication direction according to the position of the communication receiver during each scan. Hence, during each radar illumination, the system carries out a target-tracking task and simultaneously maintains the communication symbols transmission toward the intended communication direction. The simulation results verify the effective performance of the proposed approach in terms of target detection and tracking performance and angular bit error rate (BER). Furthermore, the proposed amplitude phase-shift keying signaling strategy can transmit different communication symbols to different users located within the sidelobe region and also provides a significant improvement in data rate transmission and BER performance compared with the existing sidelobe-based communication strategies.

CAMBRIDGE UNIVERSITY PRESS

Introduction

The limited availability and increasing competition for precious spectral resources among radio frequency (RF) modalities is a challenge. This problem tends to be worse since new applications are growing and their demand for spectrum keeps increasing so that it can provide new services with high quality to higher densities of users [1, 2]. There is a strong demand for joining radar and communication functions without degrading the performance of each function to make the RF spectrum usage more efficient with minimum requirements for the installation process and reduction in the hardware cost [3, 4]. In many applications, integrating radar communication functions into a single platform and moving away from independent systems design to a single platform design can be useful [5]. This has pushed extensive challenges to devise approaches to facilitate spectrum sharing between radar and wireless communication systems [1, 2]. There are two approaches to achieve spectrum sharing. The first approach has been focused on the shared spectrum access management using cognitive mechanisms [6–8] and interference mitigation techniques [5, 9]. The second approach has been concentrated on enabling the two functions to operate on the same RF platform where waveform and platform jointly design and optimize for both functions [10, 11].

The dual function radar-communication (DFRC) co-design approach has received much attention in recent years [12]. DFRC systems are capable of performing radar and communication functions concurrently using the radar's resources such as transmit platform, high transmit power, transmit waveforms, and spectral resources to achieve both functions. Since the radar's operating resources are shared for both operations, it is assumed that the primary function of the DFRC system is to fulfill a radar emission and simultaneously allowing information transmission function during the same radar pulse as a secondary function [13, 14]. The authors utilize the radar sidelobe (SL) levels to perform the communication function. Employing multiple-input multiple-output (MIMO) configuration into DFRC system designs, where the system can transmit multiple orthogonal waveforms simultaneously, would provide a waveform diversity (WD) property for the DFRC systems. Utilizing both the space-division multiple access and WD, the DFRC system is developed to detect the target within the main lobe directions while transmitting communication symbols within the SL directions of the

transmit beampatterns (BPs) radiations [14–16]. The authors in [14] used amplitude-shift keying (ASK) to modulate the SL levels where each power level represents a distinct communication symbol. Likewise, the authors in [15] used phase-shift keying (PSK) to embed the information bits as the phases of the signals transmitted toward the intended communication receiver located within the SL directions. Remarkably, the embedded information via the PSK strategy can be reliably decoded by the communication receiver located within the main beam directions. Therefore, multi-user transmission can be achieved by changing the SL levels at different angles. To avoid any degradation in the radar performance, the BP invariance approach has been adopted in [17, 18] where the embedding of the information bits is achieved via shuffling the transmitted signals across the antenna elements. Thus, the permutation matrices would contain embedded communication symbols. However, in the aforementioned approaches, a communication symbol is typically embedded into one or many radar pulses, which leads to a low data throughput that depends upon the pulse repetition frequency of the radar. Besides, the SL embedding strategies can only operate if the communication receiver is benefiting from a line-of-sight (LoS) channel. The received symbol in the multi-path channel will be significantly distorted due to the dispersed signals coming from non-LoS paths.

To increase the transmission symbol rate, frequency hopping codes were introduced in [19]. Another approach is presented in [20], where the authors proposed a two-stage far-field radiation design. In [21], the authors developed a method for communication throughput enhancement of the DFRC system by exploiting the silent period (when the primary radar function is inactive) for information transmission. However, the limitations with these approaches are: (i) there is a loss in transmit power for radar operation; (ii) communication receivers must be located within the SL directions of the radar.

The frequency diverse array (FDA) has been utilized in the DFRC system design [22, 23]. FDA radar uses a small frequency offset across the array elements and an angle-range-time-dependent BP is obtained [24]. Thus, the FDA provides extra degrees of freedom in the range dimension that the system is able to resolve the targets with different ranges even if they are at the same angle. In [23], the authors employed Costas hopping signals for the DFRC system design. The system used the construction algorithm to generate the Costas hopping waveforms, and then the information bits are embedded in each waveform using the phase modulation. However, phase synchronization is required for the proposed approach which can be a challenge to implement. To overcome this limitation, the authors in [25] utilized the phase-rotational invariance method to embed the information bits into the radiations. This approach is based on designing the transmit beamforming (BF) vectors such that each BF vector exhibits the same BP but provides a distinct phase profile. The proposed system in [22, 23] concurrently carries both radar signals and information bits in the active transmission of the radar which leads to reduced signal-to-noise ratio (SNR) and low data throughput. To improve the SNR and mitigating the cross-interference, the authors in [26] utilized the concept of SL manipulation in which they exploited the orthogonality beam property associated with the Butler matrix. In [27], the authors developed a closed-loop design into the DFRC system for enhancing the communication throughput. However, all of the aforementioned proposed signaling strategies are developed to transmit the same information bits toward the communication receivers, i.e. broadcasting transmission mode.

In this paper, we proposed a feedback-loop design for the DFRC system. It performs tracking tasks for the moving targets as a primary function and simultaneously transmitting the communication symbols toward communication directions as a secondary function during each scan. The joint transmit platform (JTP) is composed of M antenna elements where the transmitted waveforms from each element are orthogonal to each other. At the radar receiver, the predicted position information of the moving target is computed using a position predictor algorithm. This information is fed to the transmitter side in which the prior known location of the communication receiver is compared with fed back information. Accordingly, the transmitter selects a suitable information embedding scheme and appropriate BF weight vectors for both functions in the subsequent scanning. We used two information embedding schemes, namely, amplitude phase-shift keying (APSK) and PSK that one will be selected by the transmitter according to the position of the communication receiver either in the SL or main lobe directions, respectively. Moreover, the proposed APSK scheme allows different communication symbols to be transmitted to different users. The performance of the proposed system is analyzed along with simulation results. The contributions of this work can be summarized as follows:

(1) We developed a feedback-loop design for the DFRC system that allows the moving target to be tracked and maintaining the information transmission toward the intended communication directions during each illumination.
(2) We designed two information embedding schemes that utilize the amplitude and/or phase of the transmitted waveforms. This maintains the communication link toward the intended communication receiver during tracking operations.
(3) The proposed APSK information embedding strategy outperforms the existing SL-based strategies in terms of data rate transmission. It also allows different communication symbols to be transmitted to different users located within the SL directions.

The rest of the paper is organized as follows. The proposed design for joint radar communication is described in "Proposed DFRC system design" section. "Simulation results" section provides the simulation results along with performance evaluation. Finally, conclusions and future work are presented in "Conclusion and future work" section.

Proposed DFRC system design

Figure 1 depicts the functional blocks of the proposed system design. The receiver side includes the radar's receiver, memory, and position predictor blocks, while the transmitter includes five sub-blocks that contain signaling strategy selector, memory, transmit BF weight vectors design, selector of the optimum weight vectors for transmission and lastly the JTP [27]. A feedback loop design embodies the transmitter, receiver, and operational environment.

Once the DFRC system interacts with the environment, the JPT transmits orthogonal waveforms to the radar environment which involves moving target and intended communication receiver located at θ_t and θ_i, respectively. The radar receiver estimates the target parameters such as DOA and velocity exploiting the reflected signals from the environment. It is worthy to mention that, from the initial scans, a library is built which contains
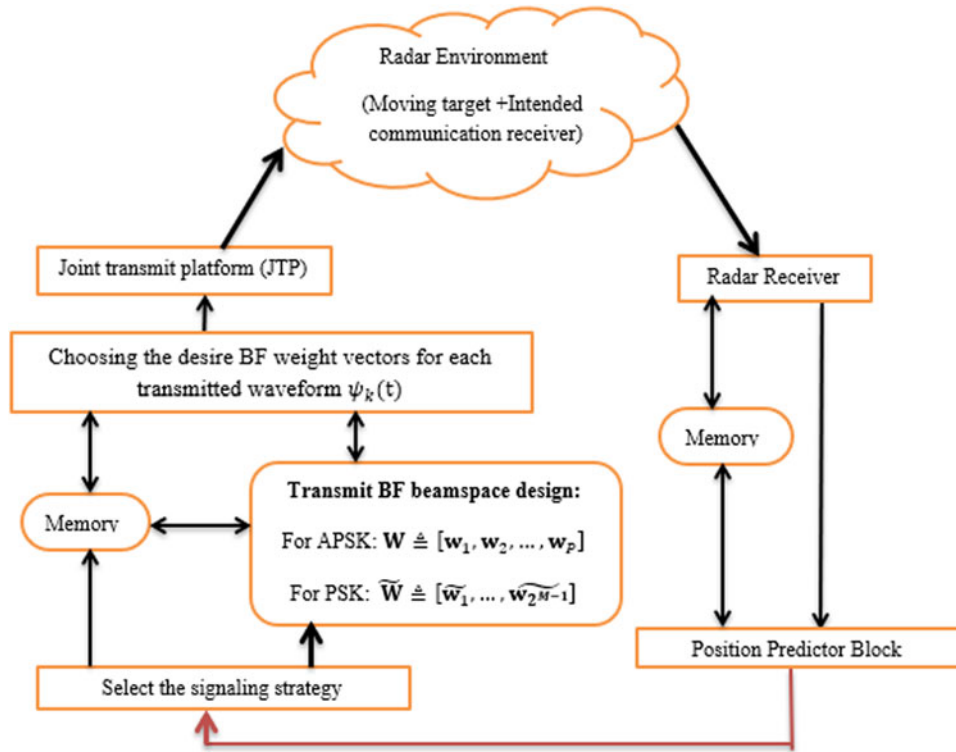
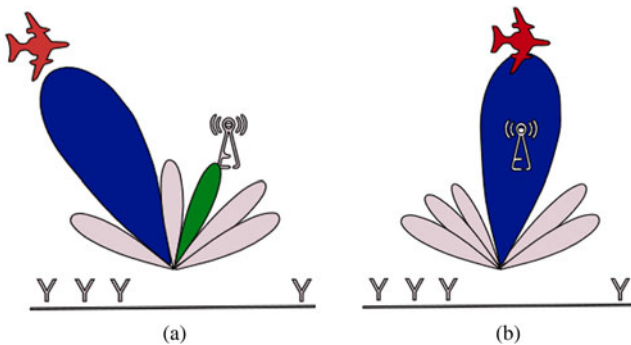**Fig. 1.** The proposed feedback-loop diagram for the DFRC system.

Fig. 2. The location of the communication receiver within the radar transmit BPs directions, (a) the communication station is located within the SL and (b) both the communication receiver and radar target are located within the main lobe.

the previous and updated estimations of target parameters and is stored in the memory. The estimated target position at **nth** time, $\widehat{P_n}$, is directed to the prediction position block to estimate the next position at $(n+1)th$ time, i.e. $\widehat{P_{n+1}}$. Next, the receiver feeds back the $\widehat{P_{n+1}}$ to the transmitter, where it compares the known location of the communication receiver with $\widehat{P_{n+1}}$. Here, there are two scenarios regarding the position of the communication receiver as shown in Fig. 2. In the first scenario, the communication receiver is located outside the main lobe directions as shown in Fig. 2(a), then the transmitter selects the proposed APSK scheme for information embedding. Whereas in the second scenario, when the receiver remains within the main beam directions as shown in Fig. 2(b), the transmitter selects the PSK scheme, where the communication symbols are embedded exclusively in the phases of the transmitted waveforms. Thus, the information transmission toward the communication

receiver is maintained during each illumination [27]. Note that, the transmitter and the receiver are co-located, therefore we assume that the feedback is always stable. In the following, we discuss each part of the design diagram independently.

Waveform model

Consider a DFRC platform with a common transmit antenna array consists of M radiating elements displaced as a uniform linear array (ULA) configuration with an inter-element spacing of d_T. Let $\{\psi_k(t)\}$, $k = 1, \ldots, K$, be the possible unity-energy transmit radar waveforms and they are orthogonal to each other, such that

$$\int_T |\psi_k(t)|^2 dt = 1, \text{ and}$$

$$\int_T \psi_k(t)\psi_{k'}^*(t) \, dt = 0, \text{ for } k \neq k'. \tag{1}$$

where T and t denote the time duration of the radar pulse and the fast time, respectively, and $(.)^*$ denotes the complex conjugate operator. It is assumed that the co-located radar receiver consists of N receive antennas array with a ULA shape and an inter-element spacing of d_R. It is further assumed that a target in the far-field would be seen by transmitting and receiving arrays from the same angle.

At the input of the JTP, the baseband representation of the transmitted signals is expressed as:

$$s(t, \ \tau) = \sqrt{\frac{E}{K}} \sum_{k=1}^{K} w_k^* \ \psi_k(t) \tag{2}$$

where τ denotes the pulse number, E is the total transmitted energy, and $\boldsymbol{w}_k$ is the kth transmit BF weight vector. Note that, the total energy E is distributed equally among K waveforms so that during one radar pulse the transmitted energy equals to E. The signals in (2) can be rewritten as:

$$s(t,\ \tau) = \sqrt{\frac{E}{K}}\ \boldsymbol{W}^* \ \boldsymbol{\Psi}(t), \tag{3}$$

where $\boldsymbol{W} \triangleq [\boldsymbol{w}_1, \boldsymbol{w}_2, \ldots, \boldsymbol{w}_k]$ is the $M \times K$ transmit beamspace matrix and $\boldsymbol{\Psi}(t) \triangleq [\psi_1(t), \ldots, \psi_k(t)]^T$ is the $K \times 1$ orthogonal waveforms vector.

The $N \times 1$ vector of the received array observations from far-field at an angle θ_t, assuming that the target of interest is located at θ_t, can be expressed as:

$$\begin{aligned}\boldsymbol{r}(t; \tau) &= \alpha_t(\tau)\big[\ \boldsymbol{a}^T(\theta_t)\boldsymbol{s}(t, \tau)\big]\boldsymbol{b}(\theta_t) + \boldsymbol{n}(t; \tau)\\ &= \sqrt{\frac{E}{K}}\ \alpha_t(\tau)\big[\ (\boldsymbol{W}^H\boldsymbol{a}(\theta_t))^T\ \boldsymbol{\Psi}(t)\big]\boldsymbol{b}(\theta_t) + \boldsymbol{n}(t; \tau),\end{aligned} \tag{4}$$

where $\alpha_t(\tau)$ is the reflection coefficient of the tth target which assumed to obey the Swerling-II model, $(.)^T$ stands for the transpose operator, and $\boldsymbol{n}(t;\tau)$ is the $N \times 1$ zero-mean white Gaussian noise vector over the τth radar pulse. Generally, $\boldsymbol{a}(\theta)$ and $\boldsymbol{b}(\theta)$ denote the radar steering vectors of transmitting and the receiving arrays in the angle θ and are defined respectively, as:

$$\boldsymbol{a}(\theta) = \big[1, e^{jk_0 d_T sin\theta}, \ldots, e^{jk_0(M-1)d_T sin\theta}\big]^T, \tag{5}$$

$$\boldsymbol{b}(\theta) = \big[1, e^{jk_0 d_R sin\theta}, \ldots, e^{jk_0(N-1)d_R sin\theta}\big]^T, \tag{6}$$

where $k_0 = \frac{2\pi}{\lambda}$ represents the wavenumber and λ is the wavelength which is defined as $\lambda = \frac{c}{f_c}$, where c and f_c denote the light speed and the carrier frequency, respectively. Then, by matched-filtering, the $\boldsymbol{r}(t; \tau)$ to the $\boldsymbol{\Psi}(t)$, $k = 1, \ldots, K$, yields the $KN \times 1$ vector of virtual received data, that is

$$\begin{aligned}\boldsymbol{y}(\tau) &= Vec\left(\int_T \boldsymbol{r}(t; \tau)\ \boldsymbol{\Psi}^H(t)\ dt\right)\\ &= \sqrt{\frac{E}{K}}\ \alpha_t(\tau)\big[\ (\boldsymbol{W}^H\boldsymbol{a}(\theta_t)) \otimes \boldsymbol{b}(\theta_t)\ \big] + \tilde{\boldsymbol{n}}(\tau),\end{aligned} \tag{7}$$

where $Vec(.)$ is the operator that stacks the columns of a matrix into one column vector, $\otimes$ denotes the Kronecker product, and $\tilde{\boldsymbol{n}}(\tau) = Vec\big(\int_T \boldsymbol{n}(t; \tau)\ \boldsymbol{\Psi}^H(t)\ dt\big)$ is the $KN \times 1$ noise term after matched-filtering and modeled as additive Gaussian with zero mean and variance $\sigma^2\ \boldsymbol{I}_{KN}$, where $\boldsymbol{I}_{KN}$ is the identity matrix of dimension $KN \times KN$.

Information embedding schemes design

In this section, we present the design of transmitting BF weight vectors and employed signaling schemes used for information embedding into radar radiation. Let $\boldsymbol{\Theta} = [\theta_{min},\ \theta_{max}]$ be the set of angles that form a spatial sector in which the radar main beam operates, i.e. where the transmitted power must be concentrate while keeping the power of the transmit emission pattern in the SL directions below a certain predetermined threshold. In the following, we present two signaling schemes used for information embedding into radar transmission.

APSK scheme

When the communication receiver is located within the radar SL directions, the DFRC system embedded the information bits using the proposed APSK-based scheme. During each radar pulse, the information embedded by controlling the amplitude levels as well as phase shifts of multiple radar waveforms radiated toward the communication directions. According to [28], the APSK scheme needs fewer amplitude levels to embed binary bits compared to the quadrature amplitude modulation (QAM) scheme. For comparison purposes, it could be seen from Fig. 3 that, the 16-QAM and 32-QAM require three and five distinct amplitude levels, respectively, to embed 4 and 5 information bits. Whereas the 16-APSK and 32-APSK only require two and three distinct amplitude levels, respectively. Since the transmit SL levels are limited, the APSK scheme is a more appropriate choice for information embedding than the QAM scheme.

The BF weight vectors for the proposed APSK scheme can be calculated by solving the following optimization problem:

$$\begin{aligned}\min_{\boldsymbol{w}_p} \max_{\theta_t} &|e^{j\mu(\theta_t)} - \boldsymbol{w}_p^H\boldsymbol{a}(\theta_t)|,\ \theta_t \in \boldsymbol{\Theta},\\ \text{Subject to } &|\boldsymbol{w}_p^H\boldsymbol{a}(\theta_s)| \le \varepsilon_{max},\ \theta_s \in \bar{\boldsymbol{\Theta}},\end{aligned} \tag{8}$$

$$\boldsymbol{w}_p^H\boldsymbol{a}(\theta_i) = A_p(\theta_i)\ e^{j\varphi_p(\theta_i)},\ p = 1, 2, \ldots, P,\ \theta_i \in \bar{\boldsymbol{\Theta}}, \tag{9}$$

where $\mu(\theta)$ is the phase profile selected by the user, $\bar{\boldsymbol{\Theta}}$ is representing the SL region, and ε_{max} is a positive number that indicates the highest allowable SL level. The above optimization problem is convex and can be solved efficiently using the convex (CVX) toolbox provided in MATLAB [29]. Here, the pth BF vector, $\boldsymbol{w}_p$, is designed to achieve the desired SL level and phase profile toward the communication direction of θ_i. Each $A_p(\theta_i)$ and $e^{j\varphi_p(\theta_i)}$, $p = 1, \ldots, P$, can assign any of the L permissible SL levels and R phases, respectively, and both are a function of angle θ_i. Figure 4(a) illustrates the 16-APSK constellation diagram applying the grey mapping to embed four bits of information. Notice from Fig. 4(a) that, the possible SL levels $L = 2$ (l_1 and l_2) while the phases $R = 5$ for l_1 and 11 for l_2. Thus, solving (9) for P times will produce all possible BF weight vectors, and the desired $\boldsymbol{w}_p$, $p = 1, \ldots, P$, that corresponding to the desired transmitted APSK symbol toward the communication receiver is selected.

In this case, the transmitted signals can be written as [27]:

$$s(t; \tau) = \sqrt{\frac{E}{K}}\ \boldsymbol{W}^* \ \boldsymbol{B}(\tau)\boldsymbol{\Psi}(t). \tag{10}$$

Here $\boldsymbol{W} \triangleq [\boldsymbol{w}_1, \boldsymbol{w}_2, \ldots, \boldsymbol{w}_P]$ is the $M \times P$ transmit beamspace matrix which includes P BF weight vectors and $\boldsymbol{B}(\tau) \triangleq [\boldsymbol{b}_1(\tau), \boldsymbol{b}_2(\tau), \ldots, \boldsymbol{b}_K(\tau)]$ is $P \times K$ selection matrix that choosing the desired BF weight vectors from $\boldsymbol{W}$ for each transmitted waveform $\psi_k(t)$, $k = 1, \ldots, K$, where $\boldsymbol{b}_k(\tau) = [b_{1, k}(\tau), b_{2, k}(\tau), \ldots, b_{P, k}(\tau)]^T$ is $P \times 1$ selection vector in which only one element in $\boldsymbol{b}_k(\tau)$ is equal to 1 and the remaining elements are zeros.

For coherent transmission mode, where the phase synchronization is required to achieve accurate detection, the transmitted embedded message toward the communication direction θ_i is
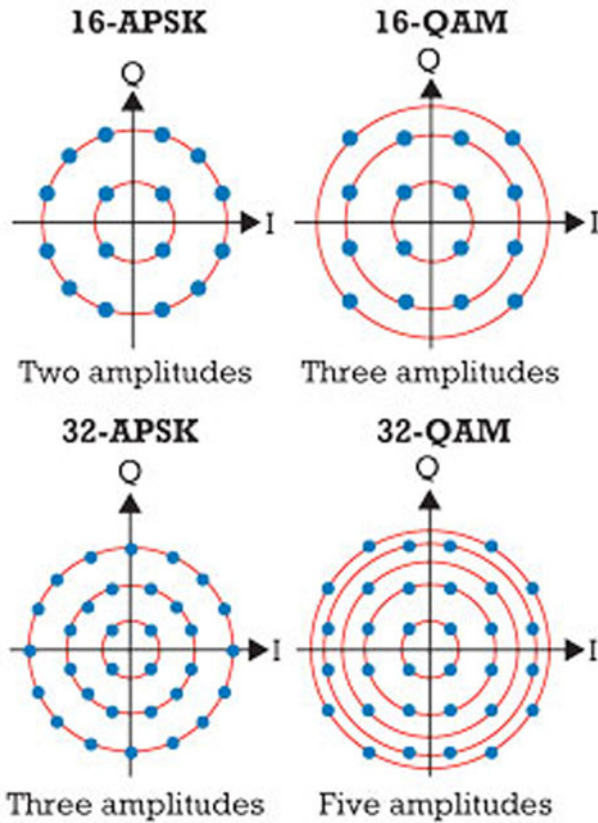
Fig. 3. Constellation schemes of the 16-QAM and 32-QAM with their counterparts in the APSK scheme.

Fig. 4. Constellation diagram with Gray coding used for embedding 4 bits of information: (a) 16-APSK scheme and (b) 16-PSK scheme.

given by

$$g_{p(APSK)}(\theta_i) \triangleq \boldsymbol{w}_p^H \boldsymbol{a}(\theta_i) = A_p(\theta_i)e^{j\varphi_p(\theta_i)}, \ 1 \leq p \leq P \leq K. \tag{11}$$

Any synchronization mismatch will result in performance degradation. To avoid this limitation, a non-coherent communication mode can be used. In this case, $\psi_1(t)$ can be selected as a reference waveform associated with $\boldsymbol{w}_1$ as reference BF weight vector. The transmitted embedded message toward the communication direction θ_i is given by

$$g_{p(APSK)}(\theta_i) \triangleq \frac{\boldsymbol{w}_p^H \boldsymbol{a}(\theta_i)}{\boldsymbol{w}_1^H \boldsymbol{a}(\theta_i)}, \ 2 \leq p \leq P \leq K. \tag{12}$$

Note that from (11) and (12), the transmitted APSK communication symbol having a magnitude component $|g_{p(APSK)}(\theta_i)|$ and phase component $angle(g_{p(APSK)}(\theta_i))$ toward the communication direction θ_i.

PSK scheme

Here, during the tracking task scenario, when the communication receiver and the target are both located within the radar main lobe region $\boldsymbol{\Theta}$. To maintain the target detection performance, a PSK-based scheme is selected by the transmitter for information embedding transmitted toward the communication receiver. According to [30], there exists $(2^{M-1} - 1)$ BF weight vectors that can be produced from the principle BF weight vector such
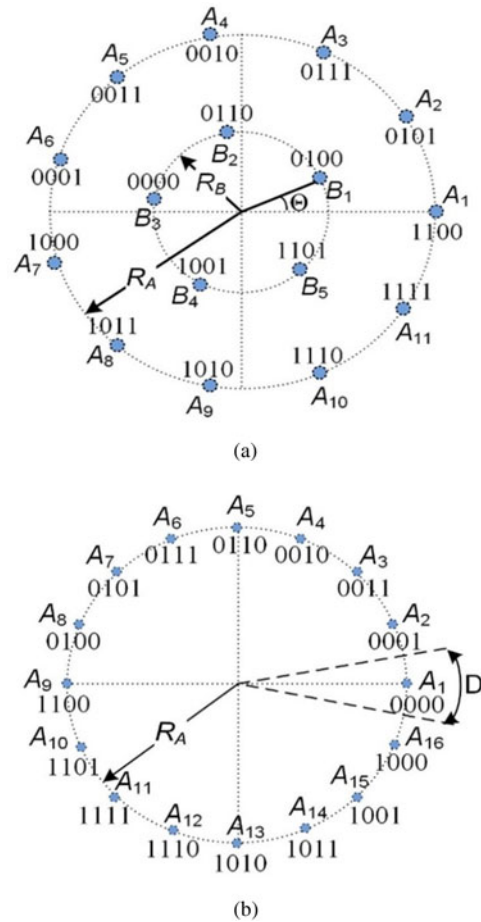
that all vectors would exhibit the same transmit BP radiation but each vector has a distinct phase profile. Therefore, if the $\widetilde{\boldsymbol{w}}_1$ is selected as the principle transmit BF weight vector from $\widetilde{\boldsymbol{W}} = [\widetilde{\boldsymbol{w}}_1, \ldots, \widetilde{\boldsymbol{w}}_{2^{M-1}}]$, which can be determined by solving the convex optimization problem as follows:

$$\min_{\widetilde{\boldsymbol{w}}_1} \max_{\theta} |e^{j\mu(\theta)} - \widetilde{\boldsymbol{w}}_1^H \boldsymbol{a}(\theta)|$$

$$\text{Subject to } \widetilde{\boldsymbol{w}}_1^H \boldsymbol{a}(\theta_t) = 1, \ \theta_t \in \boldsymbol{\Theta}, \tag{13}$$

$$\widetilde{\boldsymbol{w}}_1^H \boldsymbol{a}(\theta_i) = A \, e^{j\phi_1} \ \theta_i \in \boldsymbol{\Theta}. \tag{14}$$

Here, A is a constant value and can be set to one, and ϕ_1 represents the phase information associated with the principle BF weight vector, i.e. $\widetilde{\boldsymbol{w}}_1$. The remaining transmit BF weight vectors in $\widetilde{\boldsymbol{W}}$ can be determined using the technique developed in [25], where the information bits are embedded by controlling only the phases of the transmitted waveforms.

In this case, the signals transmitted from the JTP is given as:

$$\boldsymbol{s}(t; \tau) = \sqrt{\frac{E}{K}} \, \widetilde{\boldsymbol{W}}^* \, \boldsymbol{B}(\tau) \boldsymbol{\Psi}(t). \tag{15}$$
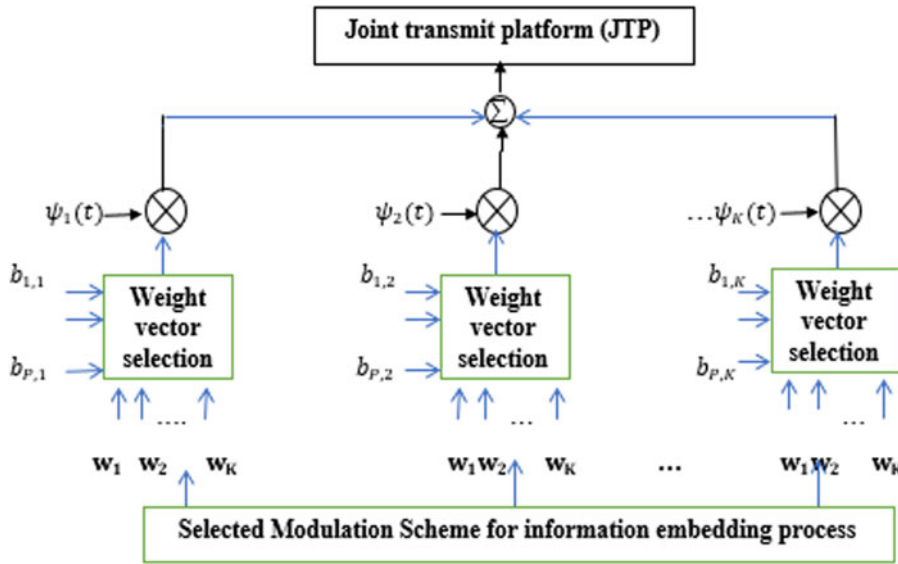
Fig. 5. Information embedding framework diagram.

Here, $\widetilde{W}$ is the $M \times 2^{M-1}$ transmit beamspace matrix while the dimension of the selection matrix $\boldsymbol{B}(\tau)$ is $2^{M-1} \times K$. The kth selection vector $\boldsymbol{b}_k(\tau)$ is with a dimension of $2^{M-1} \times 1$. Here, if 4 bits for each communication symbol are available to be transmitted toward the communication receiver, Fig. 4(b) shows the constellation scheme that is applied for the information embedding, where D represents the decision region for the communication symbol A_1.

For coherent transmission mode, the phase-embedded communication symbol transmitted toward the communication direction θ_i is given by

$$g_{k(PSK)}(\theta_i) \triangleq angle\left(\widetilde{\boldsymbol{w}}_k^H \boldsymbol{a}(\theta_i)\right) = A\, e^{j\,\phi_k},\ 1\ \leq\ k \leq 2^{M-1}$$
$$\leq K. \tag{16}$$

For non-coherent communication, $\psi_1(t)$ is selected as reference waveform along with $\widetilde{\boldsymbol{w}}_1$ as reference transmit BF weight vector via setting $\boldsymbol{b}_1(\tau) = [1,\ 0_{2^{M-1}-1}]^T$. In this case, the transmitted phase-embedded message toward the communication direction θ_i can be expressed as

$$g_{k(PSK)}(\theta_i) \triangleq angle\left(\frac{\widetilde{\boldsymbol{w}}_k^H\, \boldsymbol{a}(\theta_i)}{\widetilde{\boldsymbol{w}}_1^H\, \boldsymbol{a}(\theta_i)}\right),\ 2 \leq\ k \leq 2^{M-1} \leq K. \tag{17}$$

Notice that the transmit beamspace matrix $\widetilde{W}$ acts as the dictionary of the optimized BF weight vectors. Thus, the proposed design for the MIMO-DFRC system maintains the communication link toward the intended direction during each illumination. As a result, the overall throughput of the system is enhanced.

The information embedding framework is illustrated in Fig. 5.

Communication symbol detection
For the detection process, the communication receiver located at θ_i is assumed to have a perfect knowledge of the $\psi_k(t)$, $k = 1, 2, \ldots, K$. At the output of the communication receiver, the received signal can be written as:

$$x_i(t;\ \tau) = \alpha_{ch}(\tau)\left[\boldsymbol{a}^T(\theta_i)\, \boldsymbol{s}(t;\ \tau)\right] + z_i(t;\tau), \tag{18}$$

where $\alpha_{ch}(\tau)$ represents a complex channel response which is considered constant during τ^{th} radar pulse and $z_i(t;\tau)$ is the white Gaussian noise with zero mean and variance σ_i^2. The (18) can be rewritten as:

$$x_i(t;\ \tau) = \sqrt{\frac{E}{K}}\alpha_{ch}(\tau)\left[\sum_{k=1}^{K} g_k\ \psi_k(t)\right] + z_i(t;\tau),\ 1 \leq k \leq K, \tag{19}$$

where $g_k \triangleq \boldsymbol{w}_k^H\, \boldsymbol{a}(\theta_i)$ is the received gain associated with k^{th} BF weight vector toward the communication receiver located at θ_i. Then, by matched-filtering, the $x_i(t;\tau)$ to $\psi_k(t)$, $1 \leq k \leq K$, during each radar pulse yields

$$
\begin{aligned}
y_{i,k}(\tau) &= \frac{1}{T}\int_0^T x_i(t;\ \tau)\ \psi_k(t)\, dt \\
&= \sqrt{\frac{E}{K}}\ \alpha_{ch}(\tau)\ (\boldsymbol{w}_k^H\, \boldsymbol{a}(\theta_i)) + \widetilde{z}_i(\tau) \\
&= \sqrt{\frac{E}{K}}\ \alpha_{ch}(\tau)\ g_k + \widetilde{z}_i(\tau),\ 1 \leq k \leq K.
\end{aligned}
\tag{20}
$$

Here $\widetilde{z}_i(\tau)$ represents the output noise obtained after matched filtering and modeled as zero-mean white Gaussian noise with variance σ_i^2.

Let's define the kth received communication symbol at the communication receiver located at θ_i for coherent and non-coherent transmission modes, respectively, as:

$$s_{i,k}(\theta_i) \triangleq y_{i,k}(\tau),\ 1 \leq\ k \leq K, \tag{21}$$

$$s_{i,k}(\theta_i) \triangleq \frac{y_{i,k}(\tau)}{y_{i,1}(\tau)},\ 2 \leq\ k \leq K. \tag{22}$$

The received communication symbol would have a magnitude component and a phase component. Thus, during the tracking operation, if the intended communication receiver is located

within the SL directions then it can decode the transmitted APSK communication symbols by determining the SL levels and phases during each radar pulse as

$$\widehat{A_p} = |\, s_{i,k}\,(\theta_i)\,| \qquad (23)$$

and

$$\widehat{\varphi_p} = angle(\, s_{i,k}\,(\theta_i)\,). \qquad (24)$$

On the other hand, if the communication receiver is located within the main beam directions, then A_p in (23) is set as constant, and k^{th} embedded phase symbol, ϕ_k, via the PSK scheme can be estimated using (24) and mapped to the embedded bits.

Tracking algorithm

In tracking scenarios, a maneuvering target (MT) is considered as a non-linear dynamics system characterized by several possible operation regimes, which can be described as a sudden change in the dynamic motion equation of the system. Consequently, an MT emerges as a difficult challenge to attain track filter consistency (FC). This sort of problem is often referred to as a hybrid-state or jump Markov estimation problem [31].

One approach to deal with this type of problem is the adaptive Kalman filter (KF). For tracking MT, the adaptive KF is observing the residuals of innovations with their covariance errors in real-time, detecting a failure in FC, and adapting its parameters to retrieve FC. Unfortunately, using this approach will not provide reliable tracking performance, and this is due to the performing data association, and at the same time adjusting the filter parameters will lead to unreliable decision making [32, 33]. Another alternative approach for tracking the MT scenario is modeling the situation as the state estimation problem with Markovian switching coefficients [34]. The interacting multiple model (IMM) estimator is a typical approach for such estimation problems with Markov switching between the modes [35].

The dynamic and measurement equations for MT can be expressed as [27]

$$\boldsymbol{x}_{n+1} = \boldsymbol{F}_n(\theta_{n+1})\,\boldsymbol{x}_n + \boldsymbol{G}_n(\theta_n)\boldsymbol{v}_n(\theta_n), \qquad (25)$$

$$\boldsymbol{z}_n = \boldsymbol{H}(\theta_n)\,\boldsymbol{x}_n + \boldsymbol{w}_n, \qquad (26)$$

where $\boldsymbol{x}_n$ is the target's state vector at discrete time t_n, $\boldsymbol{F}_n$ is the transition matrix of the system, θ_n is a finite-state Markov chain with transitional probability p_{ij} of switching from mode i to mode j, $\boldsymbol{G}_n$ denotes the errors related to the state of the target. Likewise, $\boldsymbol{z}_n$ is the measurement vector at discrete time t_n, $\boldsymbol{H}$ is the measurement matrix. The random sequences $\boldsymbol{v}_n$ and $\boldsymbol{w}_n$ are mutually independent, zero-mean white Gaussian, with covariances $\boldsymbol{R}_n$ and $\boldsymbol{Q}_n$, respectively.

Therefore, the filtered state estimate $\boldsymbol{x}$ and covariance matrix $\boldsymbol{P}$ for each of r modes at a time t_n are computed for output according to

$$\boldsymbol{x}_{n\backslash n} = \sum_{i=1}^{r} \mu_n^i\,\boldsymbol{x}_{n\backslash n}^i, \qquad (27)$$

$$\boldsymbol{P}_{n\backslash n} = \sum_{i=1}^{r} \mu_n^i \left[\boldsymbol{P}_{n\backslash n}^i + (\boldsymbol{x}_{n\backslash n}^i - \boldsymbol{x}_{n\backslash n})\,(\boldsymbol{x}_{n\backslash n}^i - \boldsymbol{x}_{n\backslash n})^T \right], \quad (28)$$

where μ_n^i is the probability of regime (mode) i at discrete time t_n.

Figure 6 shows a schematic representation of IMM processing steps when $r = 2$ modes.

For many tracking systems, $\boldsymbol{x}_n$ is projected in the Cartesian system and retained stabilized in a frame of reference relative to the position of the platform. The state vector can be expressed in Cartesian coordinate's space as:

$$\boldsymbol{x}_n = \begin{bmatrix} x_n & \dot{x}_n & \ddot{x}_n & y_n & \dot{y}_n & \ddot{y}_n & z_n & \dot{z}_n & \ddot{z}_n \end{bmatrix}^T, \qquad (29)$$

where (x_n, y_n, z_n), $(\dot{x}_n, \dot{y}_n, \dot{z}_n)$, and $(\ddot{x}_n, \ddot{y}_n, \ddot{z}_n)$ denote the position, the velocity, and the acceleration components of the target at discrete time t_n, respectively.

Here, we consider two modes for the MT, namely, constant velocity (CV) and coordinated turn motion (CTM) models [36]. The CTM model characterizes the motion of MT under high acceleration maneuvers with control surfaces where the speed remains nearly constant during maneuvers. The Extended KF-IMM estimator is a typical approach for such an estimation problem [35, 37, 38].

The dynamical constraint for CV and CTM motion models can be expressed in Cartesian coordinate's space as:

$$\boldsymbol{F}_n = \begin{bmatrix} \boldsymbol{A}_n & 0_{m\times m} & 0_{m\times m} \\ 0_{m\times m} & \boldsymbol{A}_n & 0_{m\times m} \\ 0_{m\times m} & 0_{m\times m} & \boldsymbol{A}_n \end{bmatrix}, \qquad (30)$$

where $0_{m\times m}$ denotes m by m matrix of zeros and $\boldsymbol{A}_n$ is expressed for CV and CTM motions, respectively, as

$$(\boldsymbol{A}_n)_{CV} = \begin{bmatrix} 1 & \tau_n \\ 0 & 1 \end{bmatrix}, \qquad (31)$$

$$(\boldsymbol{A}_n)_{CTM} = \begin{bmatrix} 1 & \dfrac{\sin(\Omega_n \tau_n)}{\Omega_n} & \dfrac{1 - \cos(\Omega_n \tau_n)}{\Omega_n^2} \\[2ex] 0 & \cos(\Omega_n \tau_n) & \dfrac{\sin(\Omega_n \tau_n)}{\Omega_n} \\[2ex] 0 & -\Omega_n \sin(\Omega_n \tau_n) & \cos(\Omega_n \tau_n) \end{bmatrix}, \qquad (32)$$

where $\tau_n = t_n - t_{n-1}$ denotes the sampling time, t_n denotes the period of measurement n, and Ω_n represents the turn rate at a time t_n, which can be expressed as:

$$\Omega_n = \frac{\sqrt{\ddot{x}_n^{\,2} + \ddot{y}_n^{\,2} + \ddot{z}_n^{\,2}}}{\sqrt{\dot{x}_n^{\,2} + \dot{y}_n^{\,2} + \dot{z}_n^{\,2}}}. \qquad (33)$$

The input process noise covariance matrix for CV and CMT motion models is characterized by $\boldsymbol{G}_n \boldsymbol{Q}_n \boldsymbol{G}_n^T$ that is given by

$$\boldsymbol{G}_n \boldsymbol{Q}_n \boldsymbol{G}_n^T = \begin{bmatrix} q_n^x \, \boldsymbol{B}_n \boldsymbol{B}_n^T & 0_{m\times m} & 0_{m\times m} \\ 0_{m\times m} & q_n^y \, \boldsymbol{B}_n \boldsymbol{B}_n^T & 0_{m\times m} \\ 0_{m\times m} & 0_{m\times m} & q_n^z \, \boldsymbol{B}_n \boldsymbol{B}_n^T \end{bmatrix}, \qquad (34)$$

where $\boldsymbol{B}_n \boldsymbol{B}_n^T$ is expressed for CV and CTM motions, respectively, as
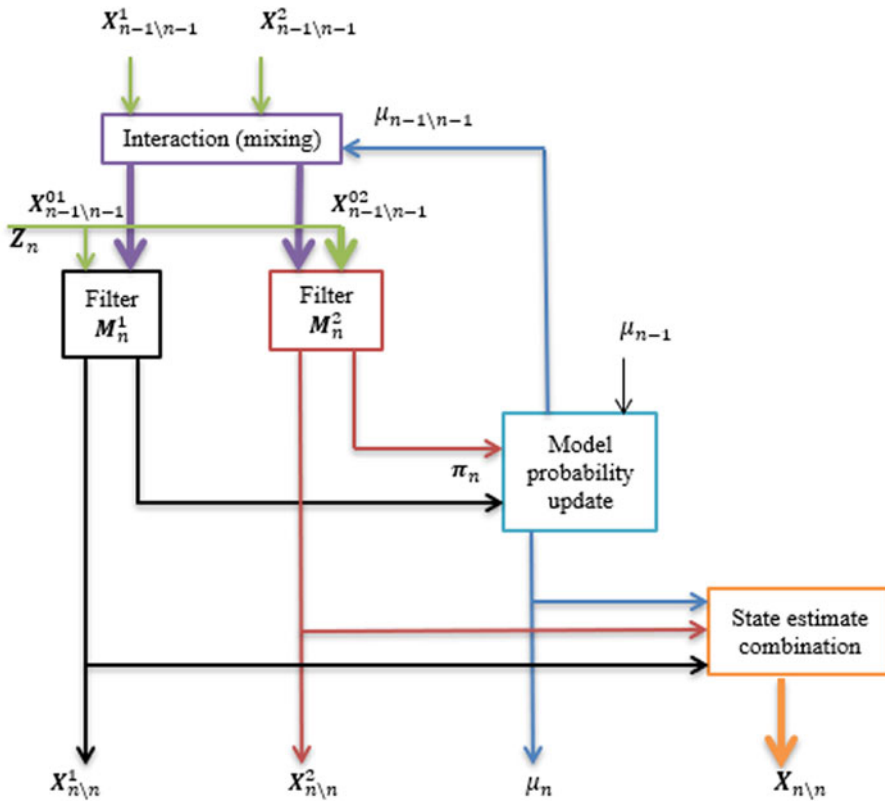
Fig. 6. Processing steps of IMM estimator with $r = 2$ modes.

$$(\boldsymbol{B}_n \boldsymbol{B}_n^T)_{CV} = \begin{bmatrix} \frac{\tau_n^4}{4} & \frac{\tau_n^3}{2} \\ \frac{\tau_n^3}{2} & \tau_n^2 \end{bmatrix}, \qquad (35)$$

$$(\boldsymbol{B}_n \boldsymbol{B}_n^T)_{CTM} = \begin{bmatrix} \frac{\tau_n^4}{4} & \frac{\tau_n^3}{2} & \frac{\tau_n^2}{2} \\ \frac{\tau_n^3}{2} & \tau_n^2 & \tau_n \\ \frac{\tau_n^2}{2} & \tau_n & 1 \end{bmatrix}. \qquad (36)$$

Simulation results

In this part of the paper, we present simulation examples to demonstrate the performance evaluation of the developed system approach. In all examples, we assume a ULA consisting of $M = 10$ antenna elements spaced $\frac{\lambda}{2}$ apart to provide information to a communication receiver located at θ_i in the radar operation regions. It is assumed that the power level in the SL region being at least 20 dB lower than the main beam is required and therefore, the maximum allowable value $\varepsilon_{max} = 0.1$ is selected.

Example 1 (Performance of the developed beamspace design in terms of a target resolution and the root mean square error (RMSE)):

In this example, the performance of the proposed optimum transmit W design approach is compared to that of the traditional MIMO radar with uniform power density transmission, and the approach presented in [39] that maps the transmit steering vector to the appropriate corresponding of a ULA based on convex optimization formulation. The main beam of the BPs is assumed to be within the spatial sector $\Theta = [-15°, 15°]$, and the number of pulses applied is 50. The probability of the target resolution and the RMSE are calculated using 500 Monte-Carlo trials. For designing the optimal W we used four beams while for the approach of [39] only two beams are used as proposed therein (see example 3 in [39]).

To investigate the RMSE performance of the approaches under test, assume that there are two targets located at $\theta_{t1} = -9°$ and $\theta_{t2} = -8°$. Here, RMSE is used as a performance criterion, which can be calculated as follows

$$\text{RMSE}(\theta) = \sqrt{\frac{1}{TM_c} \sum_{t=1}^{T} \sum_{m=1}^{M_c} (\widehat{\theta_{t,m}} - \theta_t)^2}, \qquad (37)$$

where $\widehat{\theta_{t,m}}$ denotes the estimates of the angle for the tth target in the mth Monte Carlo run, and T and M_c denote the total number of targets and Monte Carlo runs, respectively. Figure 7 shows the RMSEs versus SNR of the approaches under test. As can be seen from the figure, the RMSE of the proposed solution is lower than that of both traditional MIMO and the approach of [39].

Compared with the other approaches, the developed approach has more flexibility. In particular, the approach of [39] degrades when the number of waveforms is >2, but the developed approach can be used for any number of waveforms. To examine the resolution capability of each approach, it can be observed from Fig. 8 that the proposed beamspace design approach outperforms the other approaches under the test.
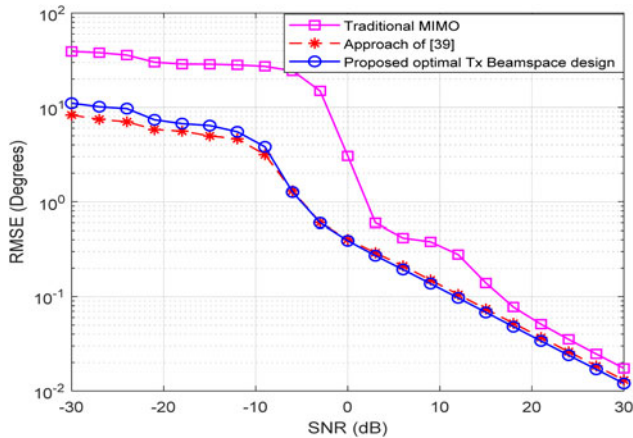
Fig. 7. RMSE performance comparison between the approaches under test, traditional MIMO, approach of [39], and the proposed beamspace design approach.
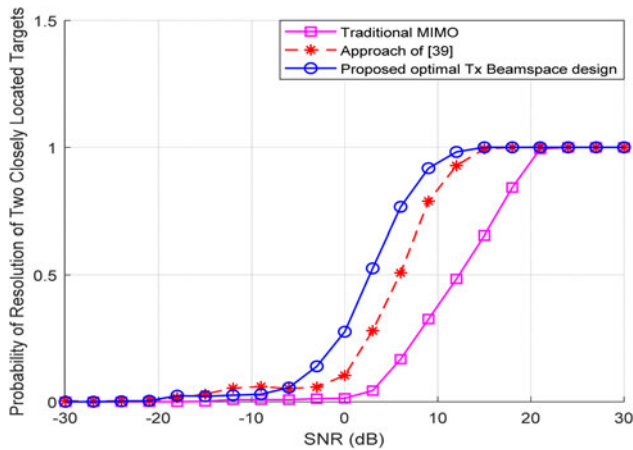

Fig. 8. Resolution performance comparison between the approaches under test, traditional MIMO, approach in [39], and the proposed optimal beamspace design.

Example 2 (Tracking of the MT):

This example illustrates the performance of tracking MT using various estimators including the proposed tracking scheme. The motion of the target is modeled as two Markov models with $\tau_n = 0.1$s and insignificant noises are used. The first model of the target motion is a linear CV with noise modeled as zero-mean with power spectral density (PSD) equal to 0.01. The second model of the motion is a combination of CV with a non-linear CTM model with noise modeled as zero-mean turn rate with covariance equal to 0.15. In the non-linear estimation problems with the multi-model approach, the EKF-IMM approach is required for filtering and smoothing. The initial simulation parameters are provided in Table 1.

The measurement z_n is made on the target position with real Gaussian noise w_n modeled as $w_n \sim \mathcal{N}(0, \Sigma_w)$ where $\Sigma_w = 0.01$ is used. The simulation is performed with 100 Monte Carlo runs, each containing 200 sampling steps and using the same generated trajectory originating from the same starting point, but the corresponding observation series are generated randomly. The actual trajectory and estimates generated by the proposed approach and different approaches in one run for filtering and smoothing are shown in Figs 9(a), 9(b), and 9(c) respectively.

Table 1. Simulation parameters used for target tracking scenario in example 2.

Parameters	Setting values
The initial state of the target x_0	$[0, 0, 1, 0, 0]^T$
The state covariance	$\text{diag}([10.1, 10.1, 1.1, 1.1, 1]^T)$
The measurement matrix H	$[1\ 0\ 0\ 0\ 0;\ 0\ 1\ 0\ 0\ 0]$
The prior probabilities model	$[0.9, 0.1]^T$
The model transition probability matrix Π	$\begin{bmatrix} 0.9 & 0.1 \\ 0.1 & 0.9 \end{bmatrix}$

For more insights, the average performance of the RMSE angle estimation over 100 Monte Carlo runs for the proposed and other estimation approaches is shown in Fig. 10.

The RMSEs of the angle parameter can be calculated as

$$\text{RMSE}(\theta_t) = \sqrt{\frac{1}{M_c}\sum_{m=1}^{M_c}(\widehat{\theta_{t,m}} - \theta_{t,m})^2}, \quad (38)$$

where M_c is the total number of the Monte Carlo runs, $\theta_{t,m}$ and $\widehat{\theta_{t,m}}$ represent the true and the estimated angle of the target in the mth run, respectively.

The RMSE of the angle parameter and average computing time per Monte Carlo run are provided in Table 2.

The proposed scheme outperforms the EKF and EK smoother using the CV model in terms of estimation accuracy but at the cost of computing speed, in which the proposed method is slower in time computation. Figure 11 shows the calculated probabilities for both modes used in this example.

Example 3 (Transmit BP synthesis when the communication station is within radar SL regions):

As mentioned above, the objective of the proposed DFRC system is tracking the distant moving target while embedding/delivering information symbols to the intended communication receiver located at θ_i in the radar operation regions. Let's assume that, the main beam of the BP is within the spatial region $\Theta = [-10°, 10°]$ and a single communication direction is located at $\theta_i = 45°$. Since the communication receiver is located outside the sector Θ, the APSK strategy is selected. Therefore, the information symbols are embedded in both the magnitudes as well as the phases of transmitted waveforms. During each radar pulse, the APSK strategy allows the transmission of L different SL levels as well as R unique phases toward the communication user by generating BF weight vectors via solving (9). Thus, each transmitted waveform carries $\log_2 LR$ bits of information to the communication user. Assuming that, two bits are embedded then the possible number of different SL levels and phase responses transmitted toward the communication direction are two. Thus, during each radar pulse, each BP of the APSK strategy corresponds to BF weight vectors that project one SL level associated with one phase response toward the communication receiver. On the other hand, for the non-coherent transmission case, W is used to build four pairs of BF vectors associated with the suitable four APSK constellation points. The transmit BP of the proposed JTP in the SL region is plotted in Fig. 12.

Example 4 (Transmit BP synthesis when communication station is within radar main beam region):

Truth
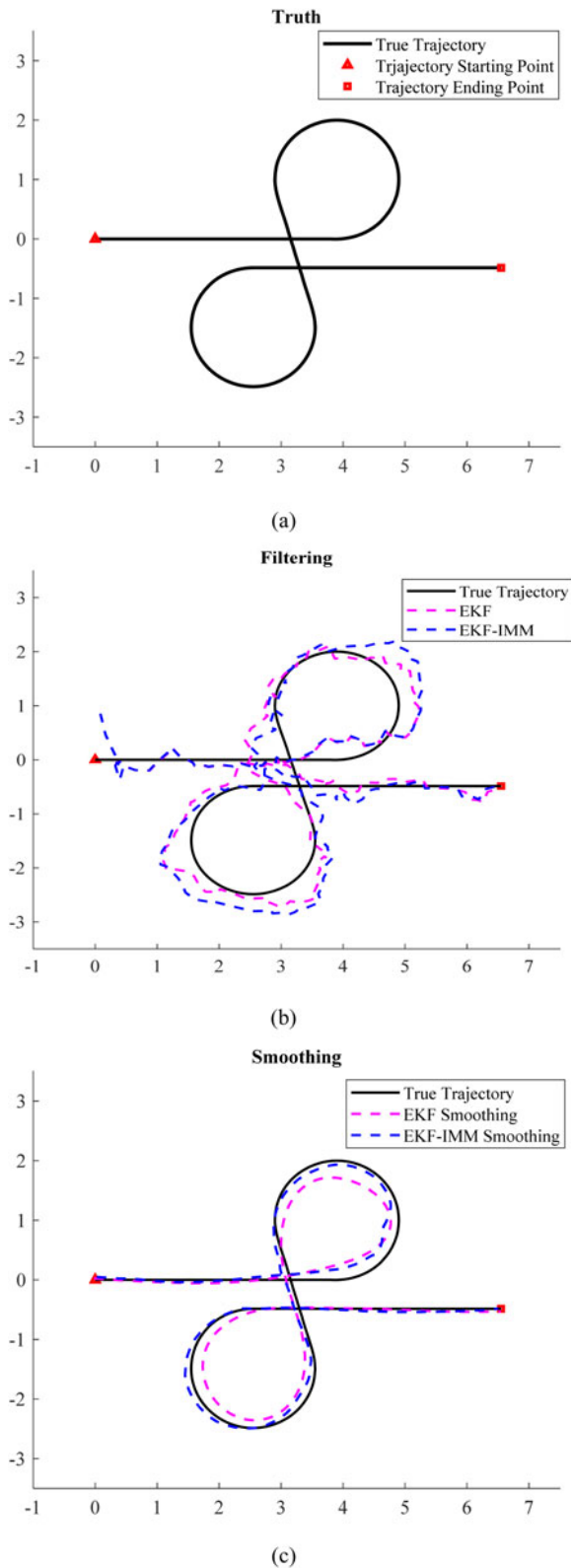

(a)

Filtering

(b)

Smoothing

(c)

Fig. 9. (a) Real trajectory, (b) estimates of the EKF and the proposed EKF-IMM filters, and (c) estimates of the EKF and the proposed EKF-IMM smoothers.

In our scenario, the main beam of the BP is moving according to the predicted position of the moving target during the tracking operation. Accordingly, if the target is moving toward the location
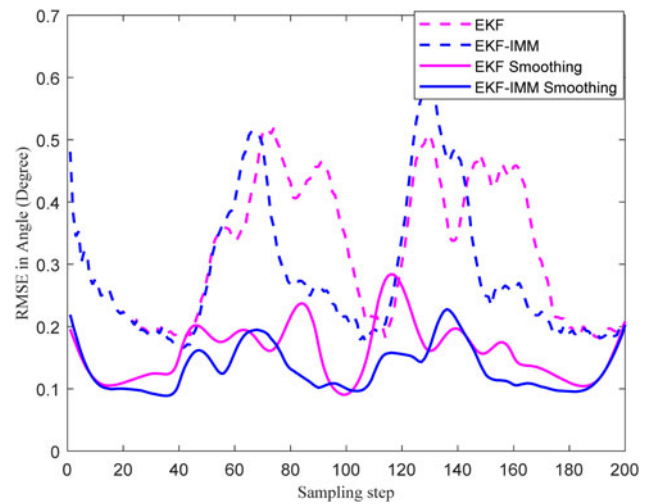

Fig. 10. RMSE in angle estimates of different non-linear filters and smoothers over sampling steps in the scenario of tracking a maneuvering target.

Table 2. Average RMSE performance for angle parameters of different non-linear estimators.

Estimators	Average RMSE of angle (degree)	Computing time (s)
EK filter (using CV)	0.3234	0.0122
EK smoother (using CV)	0.1607	0.0152
EKF-IMM	0.2860	0.0311
EKF-IMM smoother	0.1333	0.0970

of the communication station, both would be located in the radar main lobe directions. Thus, to maintain target detection performance, the information symbols are embedded only by controlling the phases of transmitted signals during each radar pulse. Again assuming that two bits of information are embedded, and accordingly, four constellation points of phases are formed and each point represents one symbol. Thus, the origin transmit BF vector $\widetilde{w_1}$ can be determined by solving (14) and the remaining BF weight vectors are selected from $\widetilde{W} = \{\widetilde{w_1}, \ldots, \widetilde{w_{2^{M-1}}}\}$ associated with each constellation point using the method presented in [25].

For a coherent PSK-based method, four BF vectors are selected from $\widetilde{W}$. On the other hand, for the non-coherent case, $\widetilde{W}$ is used to build four pairs of BF vectors associated with suitable four points of phase rotations. The transmit BP of the proposed JTP when communication direction $\theta_i \in \Theta$ during one radar pulse is plotted in Fig. 13.

Example 5 (angular bit error rate (BER)):

In this example, we examine the ability of the proposed design with an adaptive selection of information embedding strategy within the radar operation regions during each scan. The same parameters in examples 3 and 4 are used except that assuming the intended communication receiver is located at $\theta_i = 30°$ at the beginning of the tracking operation and an additive white Gaussian noise channel and SNR of 15 dB.

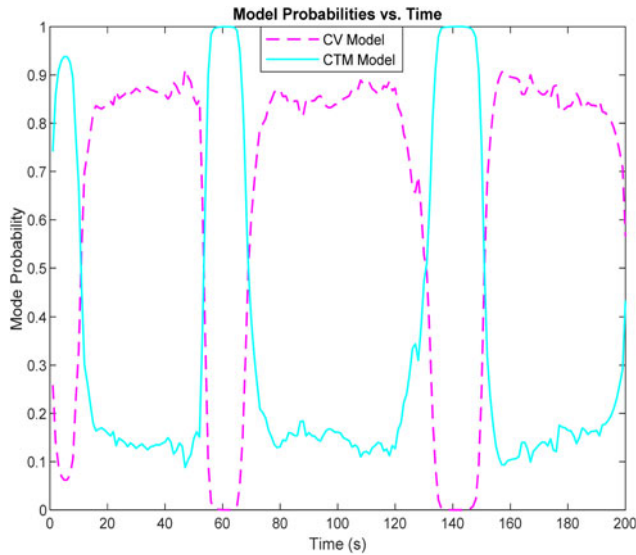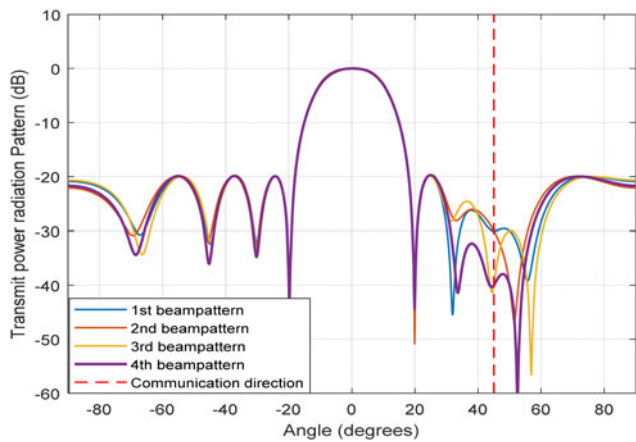The APSK communication-based strategy is selected for information embedding/delivering toward the communication

Fig. 12. Transmit BPs for the proposed DFRC system when APSK strategy is selected for information embedding toward the communication receiver located in the SL directions $\theta_i = 45°$.
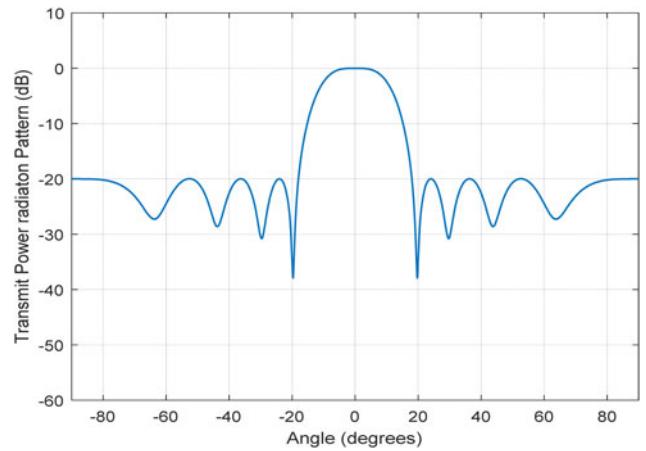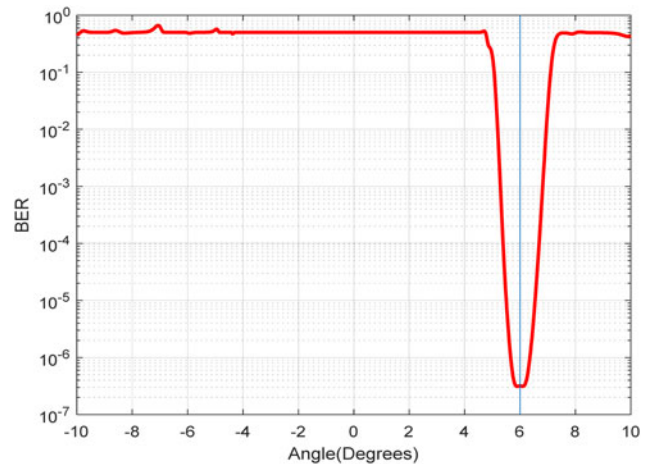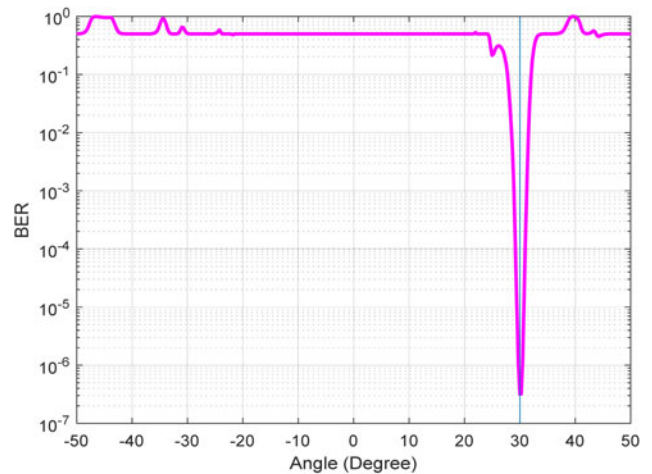

Fig. 13. Transmit BPs for proposed DFRC system applying PSK strategy for information embedding toward the communication direction $\theta_i \in \Theta = [-10°, \ 10°]$.

(a)

(b)

Fig. 14. Angular BER; when (a) the communication receiver is located at $\theta_i = 30°$ and (b) the communication receiver is located at $\theta_i = 6°$.

direction as θ_i remains outside the main beam spatial sector Θ. Figure 14(a) shows the BER versus angle for $\theta_i = 30°$ where the communication station is located. Once the moving target and communication receiver are both located within Θ directions, assuming that $\theta_i = 6°$, then the PSK is selected for information transmission toward the communication receiver so that the target detection performance and communication link are maintained. Figure 14(b) shows the BER versus angle $\theta_i = 6°$, where the communication receiver is located.

Figure 14 shows that the intended communication direction is the only direction that can receive/decipher the embedded bits reliably.

Example 6 (Transmission different information bits streams toward distinct communication users located within the SL directions):

In this example, we examined the capability of the proposed DFRC system to project different SL levels with different phase responses toward different communication stations located within

the SL region. Also, we compared the proposed APSK-based communication strategy with the existing SL-based communication strategies in terms of the overall throughput and BER performance.
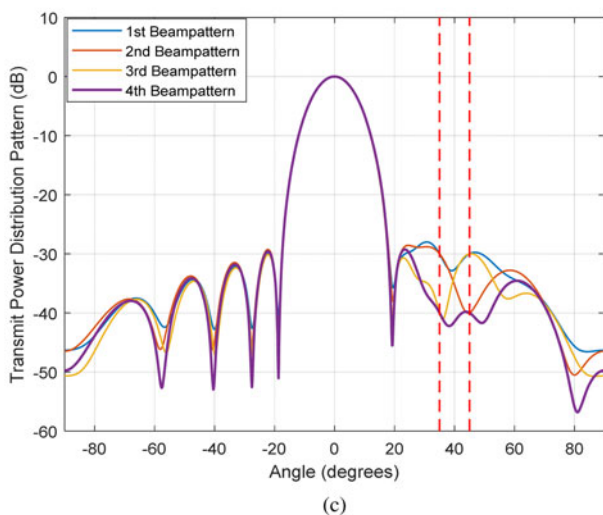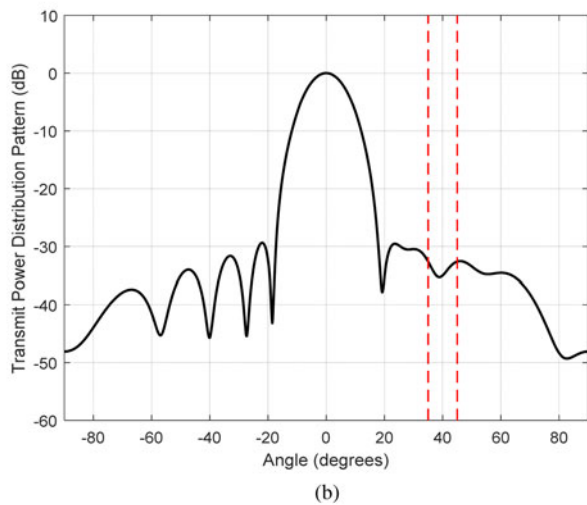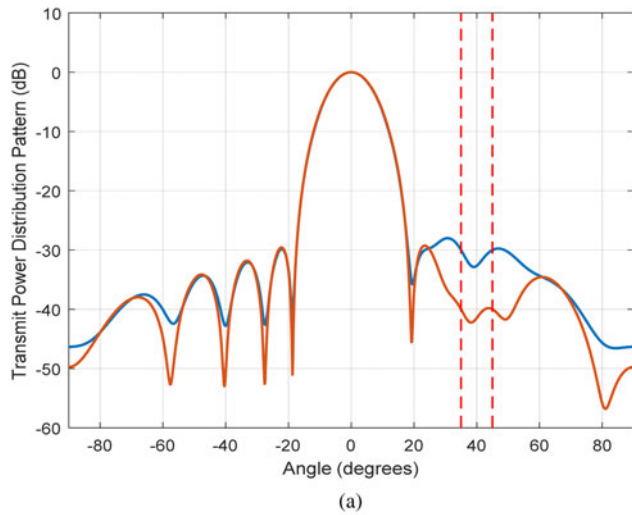
(a)

(b)

(c)

Fig. 15. Transmit BPs power radiations versus angle for various DFRC signaling strategies: (a) ASK-based communication scheme when ($L = C = 2$), (b) PSK-based communication scheme when ($R = C = 2$), and (c) proposed APSK-based communication scheme when ($L = R = C = 2$).

Here, the same simulation parameters in example 3 are used with the assumption that there are two communication receivers located at angles 35° and 45°. Assume that the secondary objective of the
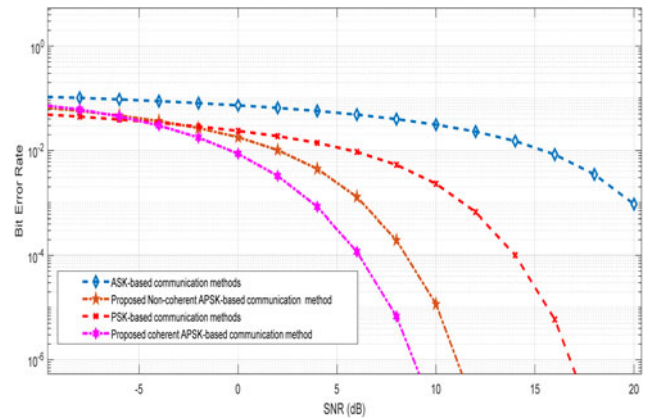

Fig. 16. BER versus SNR for various SL-based signaling strategies; ASK, PSK, and the proposed APSK schemes.

proposed system is to project two SL levels and at the same time transmit the waveforms with two distinct phases toward different communication users located at angles 35° and 45°, respectively, to embed two distinct bits of information to each user.

PSK and ASK SL-based communication strategies will have the capability to utilize only the phase or magnitude variations of the transmitted waveform, respectively. In contrast, the proposed APSK-based communication strategy can exploit the difference in both the amplitude and the phase parameters of the transmitted waveform.

Figure 15(a) shows the transmit BP radiations corresponding to two BF weight vectors for the ASK-based communication schemes [13, 14, 40, 41]. These BF vectors are designed to broadcast the SL level of either −40 or −30 dB, that is selected from $0 < L_k \leq \varepsilon_{max}$, ($k = 1, 2$), toward the communication receivers. During each radar pulse, the SL level remains identical at both communication units for the existing ASK-based communication schemes [13, 14, 40, 41]. For the PSK-based communication schemes [15, 25, 42, 43], two BF weight vectors are designed to have the same amplitude response but exhibit unique phase responses, uniformly distributed from 0° to 360°, at the communication receivers. Figure 15(b) shows that the BP radiations of these BF weight vectors have an SL level of −32.64 dB at both communication users. During each radar pulse, each of the BF vectors broadcasts a unique response of phase in the direction of all communication stations. Similar to the ASK-based communication schemes, the transmitted communication symbol is broadcast to all communication units directions.

Different from the ASK-based communication schemes, the proposed APSK-based communication scheme allows to project different SL levels at the two communication receivers. Furthermore, unlike the PSK-based communication schemes, the proposed APSK-based communication scheme, at the same time, can transmit distinct phases response to different communication receivers. Thus, the APSK-based communication scheme can independently assign two different amplitude levels and two unique phases at the two different communication directions to transmit distinct symbols to each communication user. Using (9), we generate 16 BF weight vectors for $L = R = C = 2$, where C denotes the number of communication receivers. Figure 15(c) demonstrates the four possible BPs power radiation for the proposed APSK-based communication scheme generated by using (9). Since there are two possibilities for phase responses

Table 3. Contribution comparison between the proposed system approach with ASK and PSK existing schemes approaches

Attribute	ASK-based without waveform diversity (WD)	ASK-based with WD	PSK-based	Proposed scheme design
Close-loop design	No	No	No	Yes
Information embedding within SL/main lobe	SL	SL	Either	Both
Altering the SL levels in pulse basis	Yes	Yes	No	Yes
Target position tracking	No	No	No	Yes
Multi-user transmission	No	No	No	Yes
Achievable data rate within SL region	$\log_2 L$	$K \log_2 L$	$K \log_2 R$	$K \log_2 LR$
Achievable data rate within main lobe directions	No	No	$K \log_2 R$	$K \log_2 Q$

transmitted toward each communication receiver, each BP power radiation for the proposed APSK-based communication scheme corresponds to four distinct BF weight vectors that project the identical magnitude but exhibit different responses of phases toward each communication receiver. The direction of the communication receivers is represented by the red dashed lines.

Example 7 (Data rate analysis and BER performance):

In this example, we analyze the throughput that can be achieved by each of the existing SL-based communication scheme and also evaluate their BER performance. The simulation parameters are the same as in example 6 except that there are two orthogonal waveforms will be used for transmission.

During each radar pulse, the ASK-based communication scheme exploits two SL levels and will be capable to transmit $(K\log_2 L) = 2$ bits. The PSK-based method utilizes two phases and will be able to deliver $(K \log_2 R) = 2$ bits. On the other hand, the coherent APSK-based signaling strategy can transmit $(K\log_2 LR) = 4$ bits. In the case of non-coherent communication schemes, we will have 32 BF weight vectors to be generated to achieve the same throughput. To reduce the error, Gray code is employed for all symbols in all modulation schemes before transmission.

Thus, the overall achievable throughput of the proposed APSK scheme will be

$$K \times (\log_2 LR + \log_2 Q) \times PRF \text{ bits/s,} \qquad (39)$$

where Q represents the number of bits transmitted by the system when the communication receiver is located within the Θ directions.

In the case of non- coherent communication mode, the overall achievable throughput of the proposed scheme design will be

$$(K - 1) \times (\log_2 LR + \log_2 Q) \times PRF \text{ bits/s.} \qquad (40)$$

For multi- user case, the overall achievable throughput of the proposed APSK-SL-based communication will be

$$C \times K \times \log_2 LR \times PRF \text{ bits/s.} \qquad (41)$$

Figure 16 illustrates the comparison of BER performance for the proposed APSK signaling strategy with the existing SL control-based strategies. It is evident from Fig. 16 that the proposed signaling strategy outperforms the existing SL control-based strategies in terms of BER performance. This is because the

proposed strategy is designed to increase the sum data rate with the same resources which result in a further increase of the effective distance between the transmitted symbol in the space constellation along with the ability to transmit distinct communication symbols to different receivers results in BER reduction for the proposed APSK-based signaling strategy.

Also, Fig. 16 shows that the coherent APSK-based communication mode achieves better BER performance in comparison to the counterpart non-coherent mode. This is because for non-coherent communication, the number of transmitted symbols in the constellation space is increased and since the transmitted power is divided between the waveforms resulting a higher error rate.

In short, the contribution of the developed system approach compared with the recent existing approaches is given in Table 3.

Conclusion and future work

In this paper, we have proposed an efficient DFRC system. The JTP of the system is composed of M antenna elements where the transmitted waveforms are orthogonal to each other. In this work, we proposed a closed-loop design that enables the system to perform detection and tracking of the moving target while simultaneously maintain the information transmission towards the intended communication receiver during each scan. Besides, we introduced two signaling strategies in which one of them will be selected by the transmitter according to the position of the communication receiver during the tracking operation. Thus, concerning the movement of the radar target toward or away from the location of the communication receiver, the transmitter will select PSK-based or APSK-based communication scheme, respectively. The information embedding designs have been considered for both modes of communication (coherent and non-coherent). The simulation results verify the effectiveness of the closed-loop design in terms of angular BER performance. Unlike the SL-based strategies, the proposed design allows the DFRC system to maintain the information transmission toward the communication user regardless of its location within radar regions. Moreover, the proposed APSK information embedding strategy outperforms the existing SL-based strategies in terms of data rate transmission. It also allows different communication symbols to be transmitted to different users located within the SL directions.

Ideally, the receiver of the DFRC system should be a dual function receiver, i.e used for processing the target returns and demodulating the communication symbols. In future work, the

key challenge for the receiver is to separate the target returns/echoes from the received communication signals in the presence of interference and noise.

References

1. **Griffiths H, Blunt S, Cohen L and Savy L** (2013) Challenge problems in spectrum engineering and waveform diversity, *in 2013 IEEE Radar Conference (RadarCon13)*, pp. 1–5.
2. **Griffiths H, Cohen L, Watts S, Mokole E, Baker C, Wicks M and Blunt S** (2014) Radar spectrum engineering and management: technical and regulatory issues. *Proceedings of the IEEE* **103**, 85–102.
3. **Hayvaci H and Tavli B** (2014) Spectrum sharing in radar and wireless communication systems: a review, *in 2014 International Conference on Electromagnetics in Advanced Applications (ICEAA)*, pp. 810–813.
4. **Qian J, He Z, Huang N and Li B** (2018) Transmit designs for spectral coexistence of MIMO radar and MIMO communication systems. *IEEE Transactions on Circuits and Systems II: Express Briefs* **65**, 2072–2076.
5. **Chiriyath AR, Paul B and Bliss DW** (2017) Radar-communications convergence: coexistence, cooperation, and co-design. *IEEE Transactions on Cognitive Communications and Networking* **3**, 1–12.
6. **Biglieri E, Goldsmith AJ, Greenstein LJ, Poor HV and Mandayam NB** (2013) *Principles of Cognitive Radio*. Cambridge, UK: Cambridge University Press.
7. **Wang Y** (2012) *Cognitive Informatics for Revealing Human Cognition: Knowledge Manipulations in Natural Intelligence: Knowledge Manipulations in Natural Intelligence*. Hershey, PA: IGI Global.
8. **Haykin S** (2013) Cognitive dynamic systems. In Wang Y (ed.), *Cognitive Informatics for Revealing Human Cognition: Knowledge Manipulations in Natural Intelligence*. Hershey, PA: IGI Global, pp. 250–260.
9. **Mahal JA, Khawar A, Abdelhadi A and Clancy TC** (2017) Spectral coexistence of MIMO radar and MIMO cellular system. *IEEE Transactions on Aerospace and Electronic Systems* **53**, 655–668.
10. **Zheng L, Lops M, Wang X and Grossi E** (2017) Joint design of overlaid communication systems and pulsed radars. *IEEE Transactions on Signal Processing* **66**, 139–154.
11. **Qian J, Lops M, Zheng L, Wang X and He Z** (2018) Joint system design for coexistence of MIMO radar and MIMO communication. *IEEE Transactions on Signal Processing* **66**, 3504–3519.
12. **Hassanien A, Amin MG, Zhang YD and Ahmad F** (2016) Signaling strategies for dual-function radar communications: an overview. *IEEE Aerospace and Electronic Systems Magazine* **31**, 36–45.
13. **Euziere J, Guinvarc'h R, Lesturgie M, Uguen B and Gillard R** (2014) Dual function radar communication time-modulated array, *in 2014 International Radar Conference*, pp. 1–4.
14. **Hassanien A, Amin MG, Zhang YD and Ahmad F** (2015) Dual-function radar-communications: information embedding using sidelobe control and waveform diversity. *IEEE Transactions on Signal Processing* **64**, 2168–2181.
15. **Hassanien A, Amin MG, Zhang YD and Ahmad F** (2016) Phase-modulation based dual-function radar-communications. *IET Radar, Sonar & Navigation* **10**, 1411–1421.
16. **Ahmed A, Zhang YD and Gu Y** (2018) Dual-function radar-communications using QAM-based sidelobe modulation. *Digital Signal Processing* **82**, 166–174.
17. **BouDaher E, Hassanien A, Aboutanios E and Amin MG** (2016) Towards a dual-function MIMO radar-communication system, *in 2016 IEEE Radar Conference (RadarConf)*, pp. 1–6.
18. **Hassanien A, Aboutanios E, Amin MG and Fabrizio GA** (2018) A dual-function MIMO radar-communication system via waveform permutation. *Digital Signal Processing* **83**, 118–128.
19. **Baxter W, Aboutanios E and Hassanien A** (2018) Dual-function MIMO radar-communications via frequency-hopping code selection, *in 2018 52nd Asilomar Conference on Signals, Systems, and Computers*, pp. 1126–1130.
20. **McCormick PM, Ravenscroft B, Blunt SD, Duly AJ and Metcalf JG** (2017) Simultaneous radar and communication emissions from a common aperture, part II: experimentation, *in 2017 IEEE Radar Conference (RadarConf)*, pp. 1697–1702.
21. **Al-Salehi AR, Qureshi IM, Malik AN, Khan Z and Khan W** (2019) Throughput enhancement for dual-function radar-embedded communications using two generalized sidelobe cancellers. *IEEE Access* **7**, 91390–91398.
22. **Nusenu SY, Wang W-Q and Basit A** (2018) Time-modulated FD-MIMO array for integrated radar and communication systems. *IEEE Antennas and Wireless Propagation Letters* **17**, 1015–1019.
23. **Nusenu SY and Wang W-Q** (2018) Dual-function FDA MIMO radar-communications system employing Costas signal waveforms, *in 2018 IEEE Radar Conference (RadarConf18)*, pp. 0033–0038.
24. **Antonik P, Wicks MC, Griffiths HD and Baker CJ** (2006) Range-dependent beamforming using element level waveform diversity, *in 2006 International Waveform Diversity & Design Conference*, pp. 1–6.
25. **Hassanien A, Amin MG, Zhang YD and Ahmad F** (2015) Dual-function radar-communications using phase-rotational invariance, *in 2015 23rd European Signal Processing Conference (EUSIPCO)*, pp. 1346–1350.
26. **Nusenu SY, Huaizong S, Ye P, Xuehan W and Basit A** (2019) Dual-function radar-communication system design via sidelobe manipulation based on FDA butler matrix. *IEEE Antennas and Wireless Propagation Letters* **18**, 452–456.
27. **Alselwi A, Khan AU, Qureshi IM, Khan W and Basit A** (2021) Throughput enhancement for the joint radar-communication systems based on cognitive closed-loop design. *IEEE Access* **9**, 64785–64807.
28. **Liu Z, Xie Q, Peng K and Yang Z** (2011) APSK constellation with gray mapping. *IEEE Communications Letters* **15**, 1271–1273.
29. **Grant M and Boyd S** CVX: Matlab software for disciplined convex programming, version 2.1, ed, 2014.
30. **Hassanien A, Vorobyov SA and Khabbazibasmenj A** (2015) Transmit radiation pattern invariance in MIMO radar with application to DOA estimation. *IEEE Signal Processing Letters* **22**, 1609–1613.
31. **Sworder DD and Boyd JE** (1999) *Estimation Problems in Hybrid Systems*. Cambridge, UK: Cambridge University Press.
32. **Alouani A, Xia P, Rice T and Blair W** (1991) A two-stage Kalman estimator for state estimation in the presence of random bias and for tracking maneuvering targets, *in [1991] Proceedings of the 30th IEEE Conference on Decision and Control*, pp. 2059–2062.
33. **Kirubarajan T and Bar-Shalom Y** (2003) Kalman filter versus IMM estimator: when do we need the latter? *IEEE Transactions on Aerospace and Electronic Systems* **39**, 1452–1457.
34. **Blom HA and Bar-Shalom Y** (1988) The interacting multiple model algorithm for systems with Markovian switching coefficients. *IEEE Transactions on Automatic Control* **33**, 780–783.
35. **Bar-Shalom Y, Li XR and Kirubarajan T** (2004) *Estimation with Applications to Tracking and Navigation: Theory Algorithms and Software*. Hoboken, NJ: John Wiley & Sons.
36. **Li XR and Jilkov VP** (2003) Survey of maneuvering target tracking. Part I. Dynamic models. *IEEE Transactions on Aerospace and Electronic Systems* **39**, 1333–1364.
37. **Liu H and Wu W** (2017) Interacting multiple model (IMM) fifth-degree spherical simplex-radial cubature Kalman filter for maneuvering target tracking. *Sensors* **17**, 1374.
38. **Owen MW and Stubberud AR** (2003) NEKF IMM tracking algorithm. *Signal and Data Processing of Small Targets* **2004**, 223–233.
39. **Hassanien A and Vorobyov SA** (2011) Transmit energy focusing for DOA estimation in MIMO radar with colocated antennas. *IEEE Transactions on Signal Processing* **59**, 2669–2682.
40. **Al-Salehi AR, Qureshi IM, Malik AN, Khan W and Basit A** (2020) Dual-function radar-communications: information transmission during FDA radar listening mode. *International Journal of Microwave and Wireless Technologies* **12**, 1–12.
41. **Basit A, Wang W-Q and Nusenu SY** (2020) Adaptive transmit array sidelobe control using FDA-MIMO for tracking in joint radar-communications. *Digital Signal Processing* **97**, 102619.
42. **Hassanien A, Amin MG, Zhang YD, Ahmad F and Himed B** (2016) Non-coherent PSK-based dual-function radar-communication systems, *in 2016 IEEE Radar Conference (RadarConf)*, pp. 1–6.
43. **Hassanien A, Amin MG, Zhang YD and Himed B** (2016) A dual-function MIMO radar-communications system using PSK modulation, *in 2016 24th European Signal Processing Conference (EUSIPCO)*, pp. 1613–1617.

Abdulmuneem Alselwi received his B.Sc. degree in electrical engineering from the University of Engineering and Technology (UET), Lahore, Pakistan in 2009. He is currently pursuing the Ph.D. degree in electrical engineering at International Islamic University (IIU), Islamabad, Pakistan. His research interests are in cognitive control theory, joint radar communication designs, and hybrid of multiple-input multiple-output (MIMO) with phased array and frequency diverse array (FDA) radars.
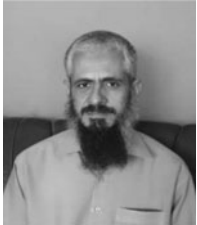
Adnan Umar Khan received the B.S. degree in electrical and electronic engineering from Eastern Mediterranean University, N Cyprus in 1994 and the M.S. degree in a communication system from the University of Portsmouth UK in 1995. He has completed his Ph.D. degree from De Montfort University UK. Currently, he is working as an Assistant Professor at the International Islamic University, Islamabad, Pakistan in the Department of Electrical Engineering. His current research interests are applying machine learning techniques to communication and power electronic problems.

Ijaz Mansoor Qureshi received the B.E. degree in avionic engineering from NED University Karachi, Pakistan, and the M.S. degree from the Department of Electrical Engineering, METU, Ankara, Turkey, in 1980. He did his Ph.D. from the University of Toronto, Canada, in 1985. He has worked as a Professor at various universities in Pakistan including Quaid-eAzam University (1987–2002), Muhammad Ali Jinnah University (2002–2007), and International Islamic University (IIU) (2007–2009). Since 2009, he has been working as a Professor and is Incharge of the graduate program with the Department of Electrical Engineering, Air University, Islamabad, Pakistan. He is also the director of the Institute of Signals, Systems, and Soft Computing (ISSS), Islamabad, Pakistan. He has around 300 publications in the various fields of engineering. His research interests are digital communication, radar signal processing, image processing, soft computing, and engineering computational mathematics.

Wasim Khan received his B.S. degree in computer engineering from COMSATS University, Abbottabad, Pakistan, in 2005. He received his M.S. and Ph.D. degrees in electrical engineering from International Islamic University, Islamabad (IIUI), Pakistan, in 2008 and 2016, respectively. Since 2009, he has been working as a Lecturer in the Department of Electronic Engineering at IIUI, Pakistan. His research interests are radar signal processing, MIMO radar, frequency diverse array (FDA) radar, and hybrid MIMO radar with phased array and FDA radar.

Abdul Basit received the M.S. and Ph.D. degrees from International Islamic University, Islamabad, Pakistan, in 2009 and 2016, respectively. He is currently working as a Postdoctoral Research Fellow with the School of Information and Communication Engineering, University of Electronic Science and Technology of China. He is also working as an Assistant Professor at an International Islamic University, Islamabad, Pakistan. His research areas include cognitive radar, frequency diverse array radar, joint radar communication designs, MIMO radar, and hybrid cognitive designs.